

# Modeling tropospheric wet delays with national GNSS reference network in China for BeiDou precise point positioning

Fu Zheng<sup>1</sup> · Yidong Lou<sup>1</sup> · Shengfeng Gu<sup>1</sup> · Xiaopeng Gong<sup>1</sup> · Chuang Shi<sup>1,2</sup>

Received: 4 April 2017 / Accepted: 13 October 2017 / Published online: 29 October 2017  
© Springer-Verlag GmbH Germany 2017

**Abstract** During past decades, precise point positioning (PPP) has been proven to be a well-known positioning technique for centimeter or decimeter level accuracy. However, it needs long convergence time to get high-accuracy positioning, which limits the prospects of PPP, especially in real-time applications. It is expected that the PPP convergence time can be reduced by introducing high-quality external information, such as ionospheric or tropospheric corrections. In this study, several methods for tropospheric wet delays modeling over wide areas are investigated. A new, improved model is developed, applicable in real-time applications in China. Based on the GPT2w model, a modified parameter of zenith wet delay exponential decay wrt. height is introduced in the modeling of the real-time tropospheric delay. The accuracy of this tropospheric model and GPT2w model in different seasons is evaluated with cross-validation, the root mean square of the zenith troposphere delay (ZTD) is 1.2 and 3.6 cm on average, respectively. On the other hand, this new model proves to be better than the tropospheric modeling based on water-vapor scale height; it can accurately express tropospheric delays up to 10 km altitude, which potentially has benefits in many real-time applications. With the high-accuracy ZTD model, the augmented PPP convergence performance for BeiDou navigation satellite system (BDS) and GPS is evaluated. It shows that the contribution of the high-quality ZTD model on PPP convergence performance has relation with the constellation geometry. As BDS constellation geometry is poorer than GPS, the improvement for BDS PPP is more significant

than that for GPS PPP. Compared with standard real-time PPP, the convergence time is reduced by 2–7 and 20–50% for the augmented BDS PPP, while GPS PPP only improves about 6 and 18% (on average), in horizontal and vertical directions, respectively. When GPS and BDS are combined, the geometry is greatly improved, which is good enough to get a reliable PPP solution, the augmentation PPP improves insignificantly comparing with standard PPP.

**Keywords** BDS · GNSS · Real-time PPP · Tropospheric modeling

## 1 Introduction

Attributed to the Real-Time Pilot Project (RTPP) and motivated by the International GNSS Service (IGS, [Dow et al. 2009](#)), IGS real-time service (RTS) was officially launched on 1 April 2013 and provides real-time official products for GPS and unofficial products for GLONASS ([Caissy et al. 2012](#); [Hadas and Bosy 2015](#)). Real-time Precise Point Positioning (PPP) has begun to receive increasing interest in studies such as early warning of earthquakes and tsunamis ([Blewitt et al. 2009](#)). However, there are still some limitations of PPP, especially in real-time kinematic applications. Among which, the long convergence time is a key factor that needs to be solved. The convergence performance of PPP is mainly affected by satellite geometry, the elimination of errors such as atmosphere delay and the pseudo-range noise. For classical PPP ([Zumberge et al. 1997](#); [Kouba 2009](#)), ionospheric-free observations are widely used in which the first-order ionospheric delay can be mitigated while the tropospheric delay is left to be estimated. In GNSS data processing, the line of sight tropospheric delay is usually expressed by the Zenith Total Delay (ZTD) of receivers with mapping functions including Niell Mapping Function (NMF, [Niell 1996](#)),

✉ Yidong Lou  
ydlou@whu.edu.cn

<sup>1</sup> GNSS Research Center, Wuhan University, 129 Luoyu Road, Wuhan 430079, China

<sup>2</sup> School of Electronic and Information Engineering, Beihang University, 37 Xueyuan Road, Beijing 100083, China

Vienna Mapping Function (VMF, Böhm and Schuh 2004; VMF1, Böhm et al. 2006a) and Global Mapping Function (GMF, Böhm et al. 2006b). The ZTD is usually expressed as the sum of hydrostatic and non-hydrostatic parts, i.e., Zenith Hydrostatic Delay (ZHD) and Zenith Wet Delay (ZWD) (Davis et al. 1985). Although ZHD can easily be modeled with the Saastamoinen model (Saastamoinen 1972) or UNB3 model (Collins and Langley 1997), the ZWD cannot be accurately modeled due to the high spatial and temporal variation of water vapor content in the atmosphere. Hence, the ZWD is usually estimated as an additional epoch-wise parameter.

For dual-frequency PPP users, under the same condition of satellite geometry and measurement noise, an accurate tropospheric model can help to accelerate the PPP convergence (Yao et al. 2017). On the other hand, a significant change in satellite geometry is required to efficiently de-correlate troposphere delay, receiver height, receiver clock and ambiguity parameters. Moreover, with poor satellite geometry, the additional ZWD parameter may result in seriously ill-conditioned solutions, while highly accurate tropospheric corrections with strong constraints can obviously improve the strength of PPP solutions. In order to improve the PPP convergence performance and avoid ill-conditioned solutions, great efforts have been made toward achieving high-accuracy tropospheric modeling.

Based on reanalysis data from the European Centre for Medium-Range Weather Forecasts (ECMWF) or the National Centers for Environmental Prediction (NCEP), several tropospheric correction models were developed. Böhm et al. (2007) established an empirical model called Global Pressure and Temperature (GPT) with spherical harmonic parameters for pressure and temperature, which has been widely applied in GNSS/VLBI/DORIS data processing. To improve the resolution in spatial and temporal variability for GPT, Lagler et al. (2013) established a new combined model GPT2, which provides mean values, annual and semi-annual variations of pressure, temperature, lapse rate, water vapor pressure and mapping function coefficients with a global regular 5° grid model. As an extension of GPT2, Global pressure and temperature 2 wet (GPT2w) was presented by Böhm et al. (2015). Compared to GPT2, GPT2w improves capability to determine zenith wet delays in blind mode with additional weighted mean temperature and water vapor lapse rate and further improves horizontal grid resolution to 1°. Furthermore, besides the annual and semi-annual variation of the climatological parameters, Yao et al. (2015) proposed an Improved Tropospheric Grid (ITG) model with consideration of the diurnal terms. As suggested by the statistical results of ZTD at 280 IGS stations, ITG and GPT2w show almost the same performance and the mean standard deviation is about 4 cm.

However, these empirical models often cause biases up to several centimeters and cannot properly reflect the actual

state of the troposphere (Yao et al. 2015), especially in severe weather conditions. In this case, it would be more appropriate to make use of high-accuracy tropospheric models, such as numerical weather models (NWM), as well as regional troposphere models based on real-time or near-real-time GNSS measurements.

Ibrahim and El-Rabbany (2011) evaluated the numerical weather prediction (NWP) model based on the National Oceanic and Atmospheric Administration (NOAA) tropospheric signal delay model (NOAATrop) and compared its performance with Hopfield (1969) within North America. The results demonstrated that the NOAATrop model was superior to the Hopfield and the PPP convergence can be improved by 1, 10 and 15% for latitude, longitude and height components, respectively. By retrieving the tropospheric delay parameters from NWM, Lu et al. (2016, 2017) and Wilgan et al. (2017) developed a NWM augmented PPP algorithm and demonstrated that the multi-GNSS PPP and real-time BDS PPP performance could be greatly improved with augmentation of global and regional NWMs. Other than the PPP augmented by NWM, there are several studies about atmospheric augmentation PPP based on the regional tropospheric model. Li et al. (2011) investigated the regional atmosphere augmentation for real-time PPP with instantaneous ambiguity resolution, in which the modified linear combination method was adopted to interpolate the user's atmospheric delays and the accuracy was about 2 cm for tropospheric interpolation. However, this method requires a bidirectional link of communication. In order to decrease the user's communication cost that results from two-way communication, Shi et al. (2014) introduced a method to determine the optimal fitting coefficients (OFCs) of local troposphere models and the results showed that the convergence performance of GPS PPP solutions, especially the height component, could be greatly improved. It is noted that the experiment in the study of Li et al. (2011) and Shi et al. (2014) was carried out in a small region, in which the maximum baseline distance was less than 200 km and the height difference was less than 26 m. With the OFCs model, de Oliveira et al. (2017) tested the local troposphere model in a larger area over France with a maximum height difference of 1651 m. The modeled ZWDs present an accuracy of around 1.3 cm with respect to the IGN (Institut National de l'Information Géographique et Forestière) final ZTD products available at: <ftp://rgpdata.ign.fr/pub/products>. The convergence performance of GPS and GPS/GLONASS PPP is improved with this local tropospheric model. Unlike for the above tropospheric model with fitted coefficients, the tropospheric correction delay in the L1-SAIF (L1 Submeter-class Augmentation with Integrity Function) augmentation of Japan QZSS is provided with a grid model. Takeichi et al. (2010) presented the strategy of this augmentation model and argued that its accuracy is 13.4 mm.

In order to promote the BDS real-time precise applications, the National BDS Augmentation Service System (NBASS) was planned for establishment in 2014. In addition, the Crustal Movement Observation Network of China (CMONOC) was established to quantify crustal deformation on the Chinese mainland. With the real-time observables from NBASS and CMONOC, it is possible to obtain a real-time tropospheric correction model for the Chinese mainland, while, regarding the studies above, the high-accuracy tropospheric delay model has been accepted as an efficient method by which to accelerate the PPP convergence for GPS and GLONASS (Lu et al. 2016; de Oliveira et al. 2017). These conclusions can hardly be applied to real-time BDS troposphere modeling across mainland China. Taking the terrain complexity of China into consideration, the real-time troposphere modeling is much more challenging. On the other hand, taking the BDS constellation into consideration, it is expected that the convergence is longer for BDS-only PPP than that of PPP with other satellite navigation systems. This is because the BDS satellite geometry varies slowly as most satellites in view are geostationary orbiters (GEO) and Inclined Geosynchronous Orbiters (IGSO). Troposphere augmentation for BDS PPP in China needs further study in detail.

In this study, some methods of tropospheric modeling adopted in the real-time application will be described. An improved troposphere model which is applicable in real-time applications will be constructed, based on evaluation of the accuracy of the models (described in Sects. 2 and 3). The contribution of this improved tropospheric model on the PPP will be analyzed in detail in Sect. 4. Meanwhile, the convergence performance of BDS and GPS PPP will be evaluated. Finally, some conclusions will be presented in the summary.

## 2 Basic model

The basic ionosphere-free observation of the GNSS can be expressed as

$$\left. \begin{aligned} P_r^s &= \rho_r^s + t_r - t^s + \alpha_r^s \cdot T_z + \varepsilon_P \\ L_r^s &= \rho_r^s + t_r - t^s + \alpha_r^s \cdot T_z - \lambda_{LC} \cdot N_r^s + \varepsilon_L \end{aligned} \right\} \quad (1)$$

in which  $P$  and  $L$  are the ionosphere-free combination of the pseudo-range and carrier-phase from receiver  $r$  to satellite  $s$  in length units, respectively. Here,  $\rho_r^s$  is the geometric distance,  $t_r$  and  $t^s$  are the receiver and satellite clock error, respectively,  $T_z$  is the zenith tropospheric delay that can be converted to slant with the mapping function  $\alpha$ ,  $N$  is the float ambiguity and the  $\varepsilon_P$  and  $\varepsilon_L$  are the measurement noise.

As discussed above, the ZTD can be calculated using empirical models such as the Saastamoinen or Hopfield model, and using the pressure and temperature with GPT.

In this study, we adopt the new model GPT2w with slant function; for more detailed information about GPT2w, we refer to Böhm et al. (2015). The ZHD can easily be modeled and the ZWD is always estimated to absorb the residual components of ZTD in data processing. For a GNSS reference network, ZWD can be generated from Eq. (1) from the reference stations with fixed coordinate (Lu et al. 2015) and then a regional tropospheric model can be developed.

In real-time GNSS applications for a large network with lots of reference stations, in order to reduce the bandwidth usage of the users, the tropospheric delays at the reference stations are usually not directly broadcast to users, but expressed as a set of fitting coefficients or corrections on a regular grid point (Takeichi et al. 2010; Pace et al. 2015). Because the ZHD can be accurately modeled by the Saastamoinen model (1972), only the ZWDs at the reference stations are involved in the real-time tropospheric modeling. In this section, two tropospheric modeling methods will be discussed. One is the local model with OFCs, and the other is the tropospheric grid point (TGP) model. Based on these models, the issue of correlation between the height and the ZWD estimation is also discussed in this section. With the consideration of the height-dependent factors in ZWD modeling, a real-time tropospheric grid point model is established. Finally, the model of PPP with tropospheric augmentation is presented for further study of the effect of real-time tropospheric model on PPP performance.

### 2.1 Local model with OFCs

The local tropospheric model with OFCs is expressed as (Shi et al. 2014):

$$\begin{aligned} ZWD_i &= a_0 + a_1x_i + a_2y_i + a_3h_i + a_4x_iy_i + a_5x_ih_i \\ &\quad + a_6y_ih_i + a_7x_i^2 + a_8y_i^2 + a_9h_i^2 \quad (i = 1, \dots, n) \end{aligned} \quad (2)$$

and the constraint equations

$$0 = \varphi_j a_j \quad (j = 1, \dots, 9) \quad (3)$$

where  $ZWD_i$  is the ZWD of the reference station  $i$ ,  $(x_i, y_i, h_i)$  represent the geodetic coordinates, and  $a_j$  are the fitting coefficients which will be estimated and broadcast to users, while  $\varphi_j$  equals '0' or '1', depending on the choice of optimal fitting coefficients. By the observation equation Eq. (2) and the constraint equations Eq. (3), the set of optimal coefficients is determined with the criterion of minimization of the square of the tropospheric fitting residuals for all the  $n$  reference stations.

In practice, the height-dependent coefficients can be removed or decreased if the height difference between the

reference stations is relatively small. In the experiment of Shi et al. (2014), the height difference between reference stations was less than 26 m and they considered the first-order fitting model with only four fitting coefficients. With dense and sparse networks in France, de Oliveira et al. (2017) adopted second-order coefficients to model tropospheric wet delays because of the large maximum height difference (1600 m). With the OFC local models, the accuracy of tropospheric modeling was about 15 mm (Shi et al. 2014; de Oliveira et al. 2017). Obviously, due to the terrain complexity with great undulations, the availability of the OFCs and the selection of the coefficients need further validation for tropospheric modeling across China.

## 2.2 Tropospheric grid point model

A general expression of the TGP model can be written as:

$$\text{ZWD}(\lambda_0, \varphi_0) = \sum_{i=1}^n w_i \text{ZWD}(\lambda_i, \varphi_i) \quad (4)$$

where  $\text{ZWD}(\lambda_0, \varphi_0)$  is the interpolated tropospheric delay at the grid  $(\lambda_0, \varphi_0)$ ,  $w_i$  denotes the weight of the ZWD for the reference station  $i$  and  $n$  is the number of stations for interpolation. Several methods can be used in the determination of the weight factor  $w_i$ , i.e., best linear unbiased estimation (BLUE) and Inverse distance weighted (IDW).

IDW interpolation explicitly assumes that things close together are more alike than those farther apart. When the IDW interpolation is adopted, the weight should be decreased with distance and determined as follows (Janssen et al. 2004):

$$w_i^{\text{IDW}} = \frac{d_{i0}^{-p}}{\sum_{i=1}^n d_{i0}^{-p}} \quad (5)$$

where  $d_{i0}$  is the distance between the estimated point and the measured point and  $p$  is a factor that denotes the weight variation with the distance. Generally,  $p$  equals '1' or '2'.

## 2.3 ZWD vertical approximation

It is widely acknowledged that the wet delay is highly correlated with altitude. Thus, no matter whether the BLUE estimator or IDW interpolation is adopted, the station height must be carefully considered in the modeling, otherwise, it may cause a bias of several centimeters (Chen et al. 2011). In order to standardize the wet delay results from these sites with different height, some methods have been proposed based on the water vapor scale height  $H$  (Elosegui et al. 1998; Kouba 2008). The wet delay at height  $h$  is expressed as

$$\text{ZWD}_h = \text{ZWD}_{\text{ref}} \cdot e^{(h_{\text{ref}}-h)/H} \quad (6)$$

where  $\text{ZWD}_{\text{ref}}$  is the wet delay at the height  $h_{\text{ref}}$  and the water vapor scale height  $H$  is about 2000 m (Kouba 2008; Yao et al. 2015).

In order to improve the accuracy of calculated wet delay, the ZWD exponential decay parameter is introduced because it can represent ZWD corrections accurately up to 10 km altitude with a reference ZWD value (Dousa and Elias 2014). Based on the UNB3 model improved by Collins and Langley (1997), Dousa and Elias propose a modified vertical approach, in which ZWD vertical dependency is a function of the water vapor pressure corresponding to the model of Askne and Nordius (1987). Instead of a water vapor pressure-decrease factor, a new parameter  $\gamma$  is introduced for the exponential decay of ZWD. The ZWD at altitude  $h$  (below 10 km) can be calculated with the  $\text{ZWD}_0$  referenced at sea level as follows:

$$\text{ZWD}_h = \text{ZWD}_0 \cdot \left(1 - \frac{\beta \cdot (h - h_0)}{T_0}\right)^{\frac{(\gamma+1) \cdot g_0}{R_d \beta}} \quad (7)$$

where  $T_0$  is the temperature at height  $h_0$ ,  $\beta$  denotes the temperature lapse rate,  $R_d$  is the specific gas constant for dry air,  $g_0$  is the gravitational acceleration and the  $\gamma$  can be fitted by way of a ZWD profile with the follow equation:

$$\frac{\text{ZWD}}{\text{ZWD}_0} = \left(\frac{P}{P_0}\right)^{\gamma+1} \quad (8)$$

From the global statistics at all heights in the study of Dousa and Elias, the new model performs better than the UNB3 model (Collins and Langley 1997), and the accuracy of the ZWD vertical estimates at different heights is better than 1 cm. For more detail of this model for calculating tropospheric delay and the results, we refer to Dousa and Elias (2014).

## 2.4 Real-time tropospheric grid point model

In real-time GNSS data processing, where in situ meteorological data is not always available, it would be more convenient to relate all the ZWDs to a reference height with an empirical model of the temperature lapse rate  $\beta$ , and  $\gamma$ . Fortunately, the GPT2w model (Böhm et al. 2015) provides mean values plus annual and semi-annual amplitudes of pressure, temperature and its lapse rate, water vapor pressure and its decrease factor, weighted mean temperature, hydrostatic and wet mapping function coefficients of VMF1, as well as the grid mean heights and geoid undulation with a horizontal resolution of 1°. By the decrease factor  $\lambda$  of water vapor pressure and the temperature lapse rate  $\beta$ , we can obtain an approximation of  $\gamma$  with the relationship introduced by Dousa and Elias (2014):

$$\lambda \cong \gamma + \frac{R_d \beta}{g_0} \quad (9)$$

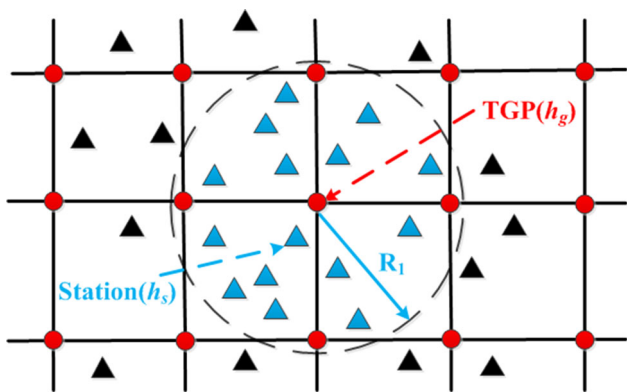


**Fig. 1** Demonstration of TGP and the stations selected for interpolation: the circle identifies the interpolation domain of the TGP. The stations (indicated by blue triangles) within this domain are characterized by having radius ( $R_1$ )

in which  $\lambda$ ,  $R_d$  and  $\beta$  can be obtained from the GPT2w model. We should note that all the parameters in the GPT2w model on a regular grid are determined at mean ETOPO5-based heights, and the geoid undulation  $h_u$  on the grid is also attached. By Eqs. (7) and (9), we can convert the  $ZWD_{h_s}$  of reference station at height  $h_s$  to the mean grid height  $h_g$ .

$$ZWD_{h_g} = ZWD_{h_s} / \left( 1 - \frac{\beta \cdot (h_s - h_u - h_g)}{T_g} \right)^{\frac{(\gamma+1) \cdot g_0}{R_d \beta}} \quad (10)$$

where  $ZWD_{h_g}$  is the ZWD value of the reference station at the mean grid height  $h_g$  and  $T_g$  is the temperature at the grid point, which can be obtained from the GPT2w model. Figure 1 shows a demonstration of reference stations and TGPs in regular grids for interpolation. The real-time ZWDs at all the stations (blue triangles) in the interpolation domain must be converted to the mean grid height  $h_g$  of the TGP by Eq. (10). Once  $ZWD_{h_s}$  at station ( $h_s$ ) is converted, the ZWDs at the TGPs can be calculated by IDW interpolation. The number of reference stations ( $N_{sta}$ ) in the interpolation domain is determined by  $R_1$ . If the  $N_{sta}$  is more than 10, we select the 10 closest stations to the grid point for interpolation. If the  $N_{sta}$  is less than ‘3’, the model value at this grid point is set to ‘0’. By effective combination of real-time GNSS observations and the GPT2w model, we can establish a Real-time Tropospheric Grid Point model of the China area, hereinafter called the RTGP model. In the RTGP model, the regular grid resolution is  $1^\circ$ , which is the same size as with the GPT2w, and the  $R_1$  is set to 1500 km.

### 2.5 PPP with tropospheric augmentation

By introducing the GPT2w model or the RTGP model, we can obtain an additional tropospheric pseudo-observation. Com-

binning this pseudo-observation and Eq. (1), the tropospheric augmentation PPP model can be written as

$$\left. \begin{aligned} \Delta P_r^s &= u_r^{sT} \Delta x_r^s + t_r + \alpha_r^s \cdot T_{ZWD} + \varepsilon_P \\ \Delta L_r^s &= u_r^{sT} \Delta x_r^s + t_r + \alpha_r^s \cdot T_{ZWD} - \lambda_{LC} \cdot N_r^s + \varepsilon_L \\ \tilde{T} &= T_{ZWD} + \varepsilon_{\tilde{T}} \end{aligned} \right\} \quad (11)$$

Furthermore, we suppose that all these observations are uncorrelated; thus, the corresponding stochastic model can be expressed as

$$D \begin{pmatrix} P \\ L \\ \tilde{T} \end{pmatrix} = \begin{pmatrix} \sigma_P^2 & 0 & 0 \\ 0 & \sigma_L^2 & 0 \\ 0 & 0 & \sigma_{\tilde{T}}^2 \end{pmatrix} \quad (12)$$

in which  $\sigma_P^2$ ,  $\sigma_L^2$  and  $\sigma_{\tilde{T}}^2$  are the variance of pseudo-range, carrier-phase and tropospheric pseudo-observation, respectively. In this study,  $\sigma_P$  is set as 0.2 m and  $\sigma_L$  is set as 2 mm, while the accuracy of the troposphere observation depends on the ZTD model.

## 3 Real-time troposphere modeling and validation

The real-time ZTD can be estimated with PPP techniques. Once ZTD estimations at the reference stations are obtained, the ZWDs can be separated from the ZTDs by calculating the ZHDs based on the GPT2w model. It should be noted that these ZWDs are subject to the residual effects of ZHDs. Based on the real-time ZWDs, the accuracy of the two methods, i.e., local model with OFCs and the RTGP model with different height-dependent parameters, will be evaluated. At the same time, the blind model GPT2w will be also evaluated with GNSS measurements.

### 3.1 Experiment details

Both the local model with OFCs and RTGP models with different height-dependent parameters are evaluated in term of ZTD accuracy; from which, a promising real-time troposphere model is proposed in this section.

With the seasonal characteristics of the troposphere delay in consideration, four weeks’ data of different seasons (winter, DOY 22–28; spring, DOY 92–98; summer, DOY 199–205; autumn, DOY 275–281) in year 2016 are collected to evaluate the accuracy of the real-time troposphere model. The distribution of stations in the experiment is shown in Fig. 2, in which the CMONOC network is used for troposphere modeling. This network is composed of 246 stations with baselines of about 100–300 km, while the NBASS network (119 stations) is used to assess the accuracy of the troposphere model. All the experimental demonstrations are

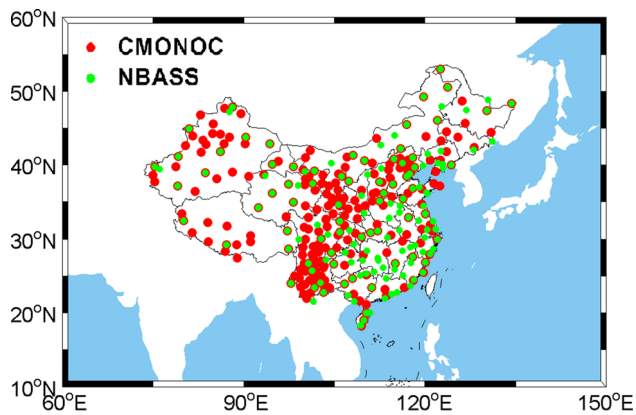


**Fig. 2** The GNSS network for troposphere modeling and validation of model accuracy

processed in real-time mode with the PANDA (Positioning and Navigation Data Analyst) software developed at Wuhan University (Liu and Ge 2003; Gu et al. 2015). Strategies used to estimate ZTDs at the reference stations are summarized in Table 1.

It is noticed that the MGEX final precise orbit and clock products are used for orbits and clock corrections in Table 1. There has been much research about real-time GNSS ZTD or precipitable water vapor (PWV) retrieval (Shi et al. 2015; Lu et al. 2015; Ahmed et al. 2016; Yu et al. 2017). It is shown that the RMS of real-time ZTD estimation is about 1 cm and there is no significant systematic error between the ZTDs with real-time and final products. However, the real-time clock quality is not always stable due to different reasons, e.g., the poor real-time streams at reference stations. In addition, the simplifications in real-time clock modeling cause accuracy attenuation for PPP users (Kouba 2009; Shi

et al. 2015). In this contribution, we focus on developing a useful, high-quality tropospheric model which is applicable for real-time applications. For convenience, instead of real-time orbit and clock product, we adopt the MGEX final orbit and clock products to simulate the processing of real-time troposphere modeling to avoid the negative effect due to the real-time clock product. In this simulated real-time tropospheric processing, the only difference with the ‘true’ real-time modeling is the final orbit and clock products used in this study.

### 3.2 Validation for local model with OFCs

As presented in Table 2, the height of the reference stations varies from several meters to several kilometers. The maximum height difference is more than 4000 m. Hence, 10 coefficients are applied in the local model with OFCs as shown in Eq. (2) and are estimated with intervals of 300 s. In general, we can evaluate the accuracy of estimations by the posterior residual of each epoch.

Figure 3 presents the 7-day RMS of the posterior residual of different seasons. As expected, the performance of the local model with OFCs varied in different seasons. Among these four seasons, the accuracy in winter shows the best performance, with a mean RMS of 1.7 cm for seven days. Figures 4 and 5 show the distribution of the posterior residuals within  $\pm 10$  cm in DOY 022 (winter) and DOY 275 (autumn) of year 2016, respectively. About 84.2% of the residual is better than 2 cm in DOY 022, but only 49.7% in DOY 275.

From analysis of the above results, it is concluded that the local model with OFCs cannot provide high accuracy in tropospheric modeling for wide areas, e.g., the Chinese

**Table 1** Processing strategies of tropospheric delay modeling and kinematic PPP

	ZTD estimation	PPP
Mode	PPP static (float solution)	PPP kinematic (float solution)
Orbits and clocks	MGEX final products ( <a href="ftp://cddis.gsfc.nasa.gov/pub/gps/products/mgex/">ftp://cddis.gsfc.nasa.gov/pub/gps/products/mgex/</a> )	
Zenith tropospheric delay	ZHD: Saastamoinen (1972) + GPT2w ZWD: Askne and Nordius (1987) + GPT2w + estimated Mapping function: VMF1 (Böhm et al. 2006a)	ZWD: constrained
Coordinates	Fixed	Estimated
Sampling	30 s	
Elevation mask	7°	

**Table 2** Station number at different height for CMONOC and NBASS

GNSS network	< 100 m	100–500 m	500–1000 m	1000–2000 m	2000–3000 m	> 3000 m
CMONOC	48	45	35	74	22	22
NBASS	31	38	11	27	6	6

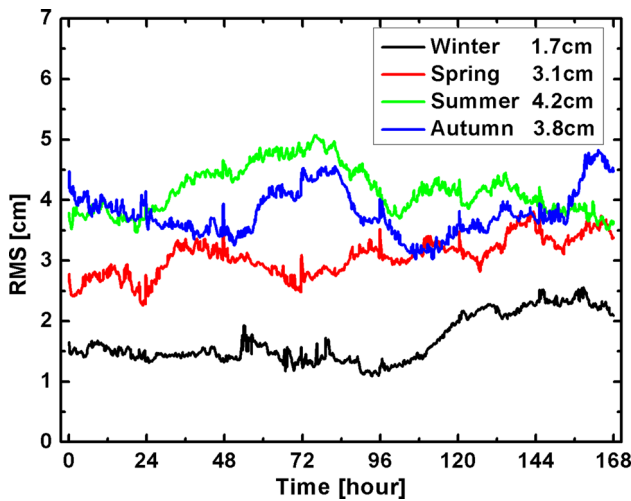


Fig. 3 RMS of the posterior residual of the local model with OFCs

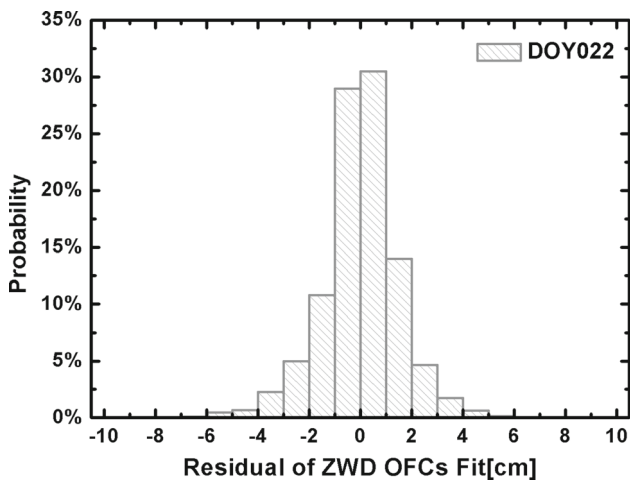


Fig. 4 Statistics of the residual of the local model with OFCs in DOY 022

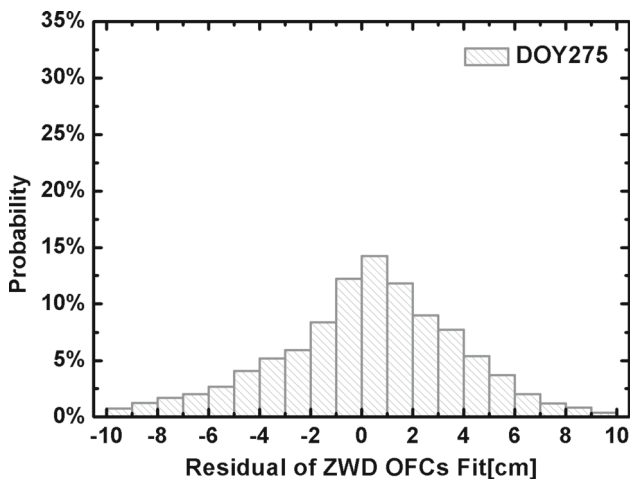


Fig. 5 Statistics of the residual of the local model with OFCs in DOY 275

mainland. This is not surprising, because the geometry of the observation equations is poor and the coefficients are very sensitive to the error of the ZWD used for modeling.

### 3.3 Accuracy of the RTGP and GPT2w models

The RTGP model is established using the IDW method after the ZWDs are converted to the corresponding grid point height. There are no posterior residuals for evaluation of the RTGP model; hence, external validations are introduced in this section. As shown in Fig. 2, the reference stations of the NBASS network are selected to evaluate the RTGP model. The real-time ZTDs at these stations are calculated by bilinear interpolation, and the reference values are calculated in post-processing mode using PANDA. The RMS and maximum value of the differences between the real-time ZTDs and the post-time ZTDs are made statistics to evaluate the accuracy of the RTGP model.

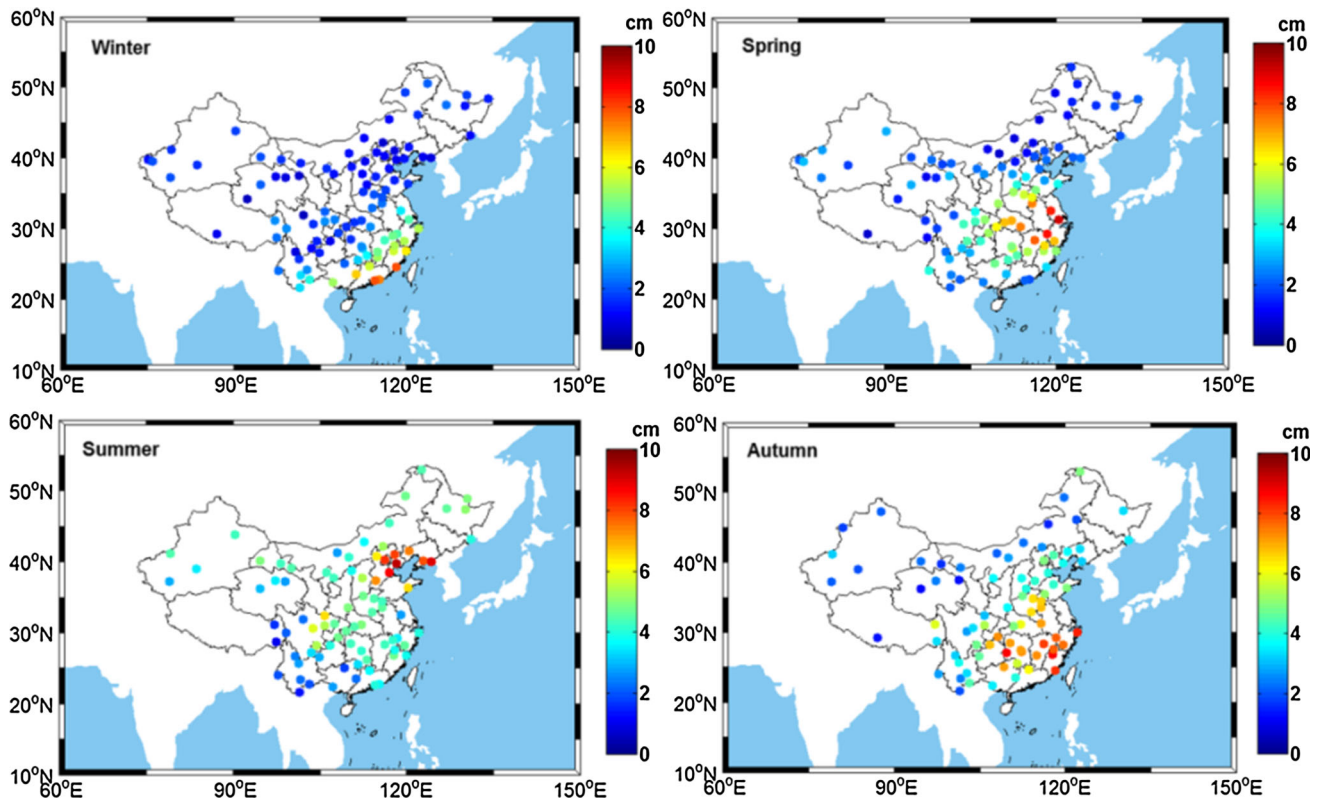
When modeling the tropospheric delay with the RTGP model, two height-dependent parameters are introduced, one is water vapor scale height, here we adopt 2000 m, and the other parameter is the modified parameter shown in Eq. (9). In addition to the RTGP model based on these two parameters, the performance of the GPT2w model over mainland China will also be evaluated.

Table 3 illustrates the RMS and the maximum values (from absolute values) of four seasons for different models. Figures 6 and 7 plot the RMS values of ZTD difference at each NBASS reference station for the RTGP model with Eq. (10) and GPT2w, respectively. The average RMS of the GPT2w model is about 3.6 cm, which is consistent with the results of Yao et al. (2015). However, the maximum of the GPT2w model is about 12 cm. As shown in Fig. 6, the GPT2w model performs worse in the coastal area than in other areas in all four seasons, the maximum value at these stations is about 10 cm. This means that it is difficult for the blind model to accurately depict the true state of the troposphere. Compared with the GPT2w model, the models with Eqs. (6) and (10) all perform better than the GPT2w model, and the model with Eq. (10) shows better performance than the model with Eq. (6). On the other hand, it is also seen that the accuracy of GPT2w and RTGP models shows significant seasonal differences for these models, with the accuracy in winter and spring being better than that in summer and autumn. For the RTGP model, the average RMS is about 1 cm in winter and spring, while about 1.5 cm in summer and autumn. It should be also noted that some stations perform worse in some cases. Especially in the autumn, the RMS can be up to 5 cm, as shown in Fig. 7.

Based on the above analysis, it is shown that the RTGP model is more suitable than the local model with OFCs for modeling the tropospheric delay in the China region. Comparing the accuracy of the RTGP model with Eqs. (6) and (10) shows that the RTGP model with the parameter introduced

**Table 3** Accuracy of the ZTD model with RTGP1 (Eq. 6), RTGP2 (Eq. 10) and GPT2w in four seasons (unit: cm)

	RMS			MAX		
	RTGP1	RTGP2	GPT2w	RTGP1	RTGP2	GPT2w
Winter	0.81	0.80	2.42	3.53	3.46	9.37
Spring	1.07	1.05	3.29	3.82	3.73	11.45
Summer	1.50	1.41	4.33	6.37	4.73	12.71
Autumn	1.42	1.39	4.33	5.09	5.09	13.49
Average	1.20	1.16	3.59	4.70	4.25	11.76



**Fig. 6** Average RMS of the GPT2w model for different periods

by the combination of GPT2w and the method of [Dousa and Elias \(2014\)](#) performs better than that with the water vapor scale height (2000 m). In order to satisfy real-time applications at different altitudes, this general parameter should be adopted. Overall, the tropospheric delay can be modeled with the average RMS of 1.2 cm. It should be noted that this tropospheric model is established with IGS final clock products in this study, the evaluation results illustrate this model can be used in real-time applications when the real-time clock product is applicable.

#### 4 Real-time PPP with troposphere augmentation

Both the real-time tropospheric model and GPT2w model can provide external corrections for PPP. From the above

analysis, it is concluded that the RTGP model performs better than the GPT2w model. In this section, by introducing the concept of Dilution of Precision (DOP), the effect of ZTD estimation on BDS/GPS PPP positioning performance is analyzed; then the contribution of the external corrections (including the RTGP and GPT2w models) on the kinematic PPP is evaluated.

#### 4.1 DOP analysis

In general, the DOP is an important index for evaluating the accuracy of positioning and timing performance, including Horizontal DOP (HDOP), Vertical DOP (VDOP), Position DOP (PDOP) and Time DOP (TDOP). In order to analyze the effect of ZTD estimation on the PPP solution (as is done for HDOP and VDOP), the DOP of ZTD is introduced in this



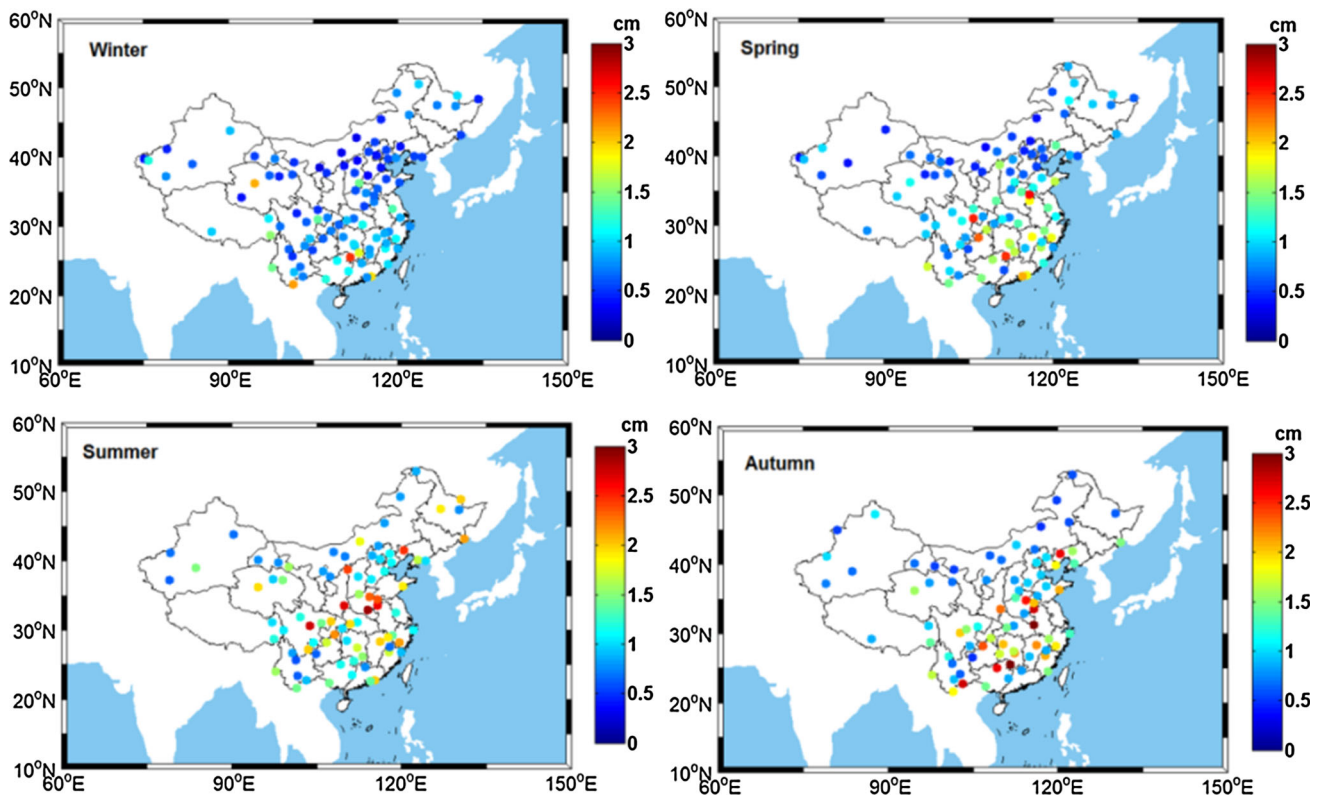


Fig. 7 Average RMS of the RTGP model for different periods

study. For convenience, we will call it TrDOP (Tropospheric DOP). In the local Cartesian coordinate system, the design matrix  $B$  is defined as

$$B = \begin{bmatrix} \cos(ele^1) \cdot \sin(azi^1) & \cos(ele^1) \cdot \cos(azi^1) & \sin(ele^1) & 1 & \alpha^1 \\ \cos(ele^2) \cdot \sin(azi^2) & \cos(ele^2) \cdot \cos(azi^2) & \sin(ele^2) & 1 & \alpha^2 \\ \cos(ele^3) \cdot \sin(azi^3) & \cos(ele^3) \cdot \cos(azi^3) & \sin(ele^3) & 1 & \alpha^3 \\ \cos(ele^4) \cdot \sin(azi^4) & \cos(ele^4) \cdot \cos(azi^4) & \sin(ele^4) & 1 & \alpha^4 \\ \vdots & \vdots & \vdots & \vdots & \vdots \\ \cos(ele^n) \cdot \sin(azi^n) & \cos(ele^n) \cdot \cos(azi^n) & \sin(ele^n) & 1 & \alpha^n \end{bmatrix} \tag{13}$$

where  $ele^i$ ,  $azi^i$  and  $\alpha^i$  ( $i = 1, 2, \dots, n$ ) are the elevation angle, the azimuth angle and the zenith wet delay mapping coefficient of the satellite  $i$ , respectively, while  $n$  is the satellite number at each epoch. Based on the design matrix  $B$  and the weighted matrix  $P$  of satellite observations, which depend on the satellite elevation angle, the covariance matrix  $Q$  is defined as

$$Q = (B^T \cdot P \cdot B)^{-1} = \begin{bmatrix} q_{11} & q_{12} & q_{13} & q_{14} & q_{15} \\ q_{21} & q_{22} & q_{23} & q_{24} & q_{25} \\ q_{31} & q_{32} & q_{33} & q_{34} & q_{35} \\ q_{41} & q_{42} & q_{43} & q_{44} & q_{45} \\ q_{51} & q_{52} & q_{53} & q_{54} & q_{55} \end{bmatrix} \tag{14}$$

The DOPs including HDOP, VDOP and TrDOP can be expressed as

$$\left. \begin{aligned} HDOP &= \sqrt{(q_{11} + q_{22})} \\ VDOP &= \sqrt{(q_{33})} \\ TrDOP &= \sqrt{(q_{55})} \end{aligned} \right\} \tag{15}$$

By comparing the variations of HDOP and VDOP after introducing the TrDOP, the effect of TrDOP on the PPP solutions will be analyzed for BDS-only, GPS-only and for BDS/GPS combined PPP, respectively. The value of TrDOP and its rate of change over time will affect the estimation of ZTD. Because the positioning error in the vertical direction has strong correlation with ZTD, it means that the value of TrDOP also has indirect impact on the PPP positioning accuracy.

Four stations (CHUN, XJKE, SCGZ and YNSM) evenly distributed over China, listed in Table 4, are selected for the analysis. Figure 8 illustrates the time series of BDS, GPS and BDS/GPS combined TrDOP at the four stations in DOY 200 of year 2016. It is presented that the BDS TrDOP is much bigger than GPS. Meanwhile, the variation of BDS TrDOP is relatively slow; for example, the BDS TrDOP at CHUN station is always close to '5' during the periods between UTC 03:00 and 07:00. The BDS TrDOP at station XJKE is different from other stations between UTC 10:00 and 14:00,

**Table 4** Mean value of TrDOP for BDS, GPS and BDS + GPS

Stations	Latitude (°)	Longitude (°)	TrDOP (BDS)	TrDOP (GPS)	TrDOP (BDS + GPS)
CHUN	43.8	125.4	4.0	1.7	1.0
XJKE	41.8	86.2	2.9	0.9	0.6
SCGZ	31.6	100.0	7.6	1.2	0.7
YNSM	22.7	101.0	9.3	1.3	0.8

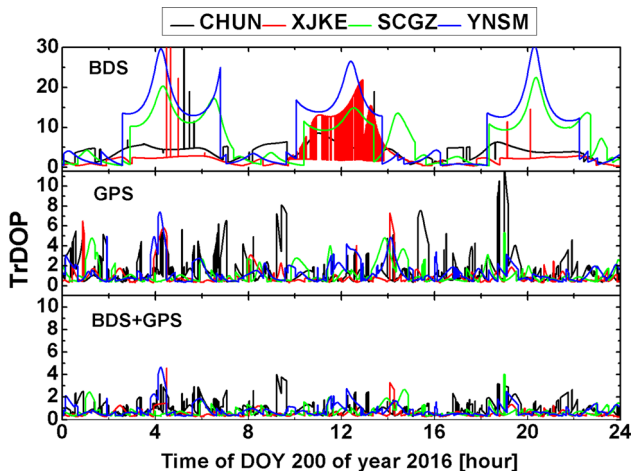


**Fig. 8** BDS, GPS and BDS+GPS TrDOPs at four stations in DOY 200 of year 2016

the TrDOP changes frequently, which results from the number of observable satellites changes. It means the TrDOP is related with the satellite geometry. Furthermore, when BDS and GPS are combined, the satellite geometry is sig-

nificantly improved, as shown in Table 4. The BDS/GPS combined TrDOP improves about 80 and 40% compared to BDS TrDOP and GPS TrDOP, respectively.

In order to analyze the effect of the ZTD parameter on HDOP and VDOP, in Fig. 9 the BDS HDOP and VDOP is plotted with and without estimation of ZTD at the stations. It is noted that the variation of VDOP with ZTD estimation is more significant than that of HODP because of the strong correlation between ZTD and the vertical positioning error. It is found that the BDS TrDOP is bigger than that of GPS and BDS/GPS in Fig. 8. Hence, for BDS PPP, the effect of ZTD estimation on the PPP solution should be bigger than that for GPS PPP. Here, we introduce a ratio to evaluate the influence of TrDOP on HDOP and VDOP, as follows

$$\text{ratio} = \frac{\text{DOP}_{\text{with ztd}}}{\text{DOP}_{\text{without ztd}}} \tag{16}$$

Using Eq. (16), the ratios of HDOP and VDOP at different stations are calculated. Figure 10 presents the ratios of the BDS, GPS and BDS/GPS for HDOP and VDOP at the stations CHUN and YNSM. It is seen that the ratio of BDS HDOP and VDOP is much bigger than that of GPS or

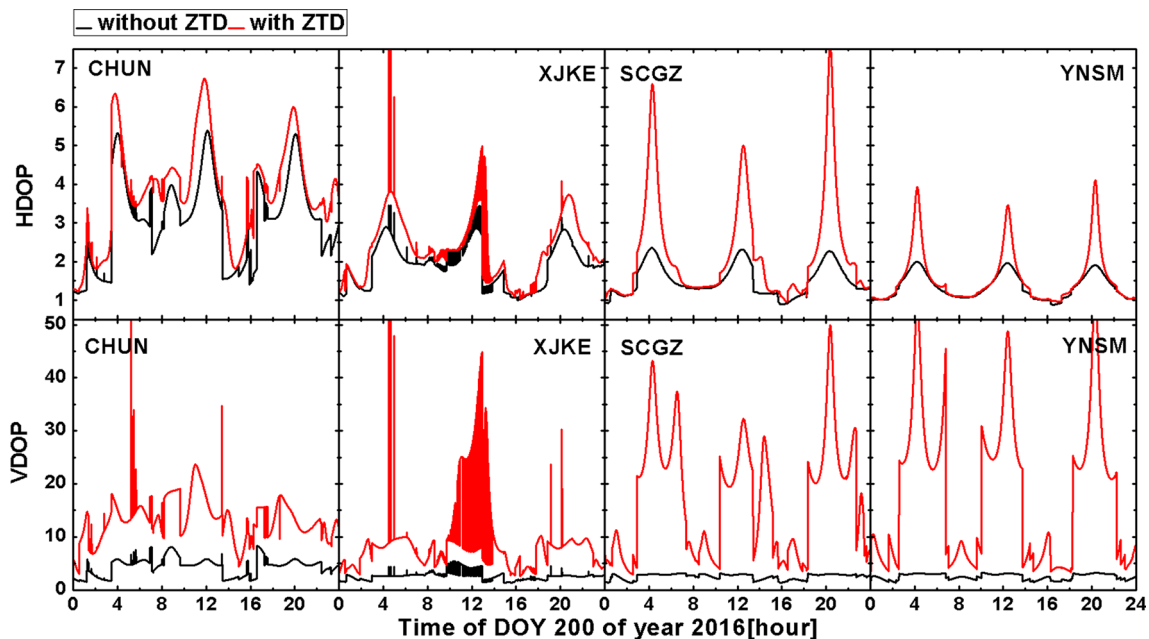


**Fig. 9** BDS HDOP and VDOP at four stations in DOY 200 of year 2016

**Fig. 10** The ratio of HDOP and VDOP at station CHUN and YNSM

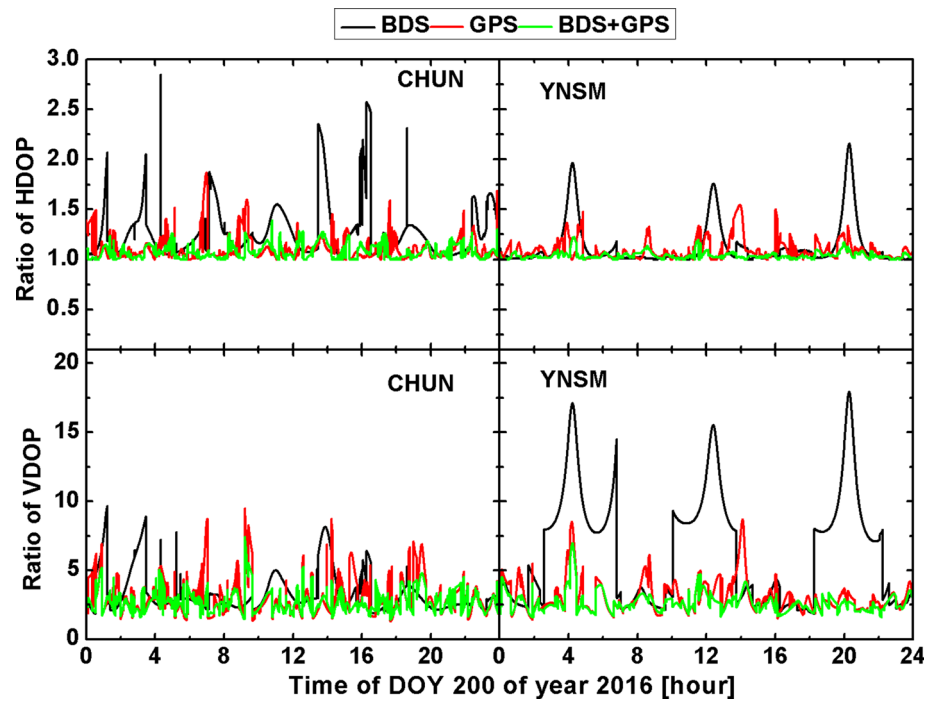


**Table 5** Mean value of ratio of HDOP and VDOP for BDS, GPS and BDS+GPS

Stations	Ratio of HDOP			Ratio of VDOP		
	BDS	GPS	BDS+GPS	BDS	GPS	BDS+GPS
CHUN	1.3	1.1	1.1	3.3	3.1	2.7
XJKE	1.2	1.1	1.1	3.4	2.7	2.4
SCGZ	1.4	1.1	1.1	6.5	3.0	2.6
YNSM	1.1	1.1	1.0	6.4	3.1	2.7

BDS/GPS, especially the ratio of BDS VDOP at the station YNSM. Table 5 lists the average ratios of the HDOP and VDOP for BDS, GPS and BDS/GPS, respectively. It seems that the estimation of ZTD has little influence on the HDOP, especially for GPS or BDS/GPS, while the VDOP becomes bigger when the ZTD is estimated. The ratio of GPS VDOP is about ‘3’ while that of the BDS VDOP is bigger, which varied between ‘3’ and ‘6’ at these four stations. On the other hand, for the BDS/GPS combined solution, the estimation of ZTD has little influence on HDOP and the ratio of VDOP is smaller than that of BDS and GPS. The VDOP has been improved, but this is not significant compared to the GPS VDOP.

On the basis of above analysis, it is concluded that the estimation of ZTD may affect the PPP solution, especially for the vertical positioning error, and this effect may be more obvious for BDS PPP. Because the BDS GEOs and IGSOs are the largest and most dominant contributions in the BDS PPP, the variation in the geometry of these satellites is rela-

tively slow, which is not conducive for the separation of the ZTD and the error in the vertical direction, and which also results in a long convergence time. When the high-accuracy ZTD model is introduced, a strong constraint on the pseudo-observation equation of ZTD will reduce the impact of the strong correlation between the ZTD and the vertical error and accelerate the initialization of the PPP solution. Hence, in order to evaluate the contribution of the RTGP model on the PPP, the PPP for BDS, GPS and BDS/GPS are processed with the RTGP model in the following section.

#### 4.2 PPP convergence analysis

In order to assess the performance of different ZTD models and their contribution on positioning, kinematic PPP with BDS-only, GPS-only and the BDS/GPS combined mode is carried out in this section. For this, the daily static solution of these stations with PANDA software is regarded as reference.

Shown in Figs. 11, 12, and 13 are the BDS-only, GPS-only and BDS/GPS combined PPP series with the GPT2w and RTGP models, respectively. It is suggested that the RTGP model can greatly reduce the convergence time compared with the GPT2w model for BDS PPP. Because the TrDOP value is larger and varies slowly at CHUN during the period of initialization, the accuracy of the ZTD estimation is low and the positioning accuracy in the vertical direction is correspondingly low. If we calculate the RMS of positioning error before convergence, we find that the accuracy of the PPP solution with the RTGP model is better than that with the GPT2w model. The improvement for BDS PPP is about

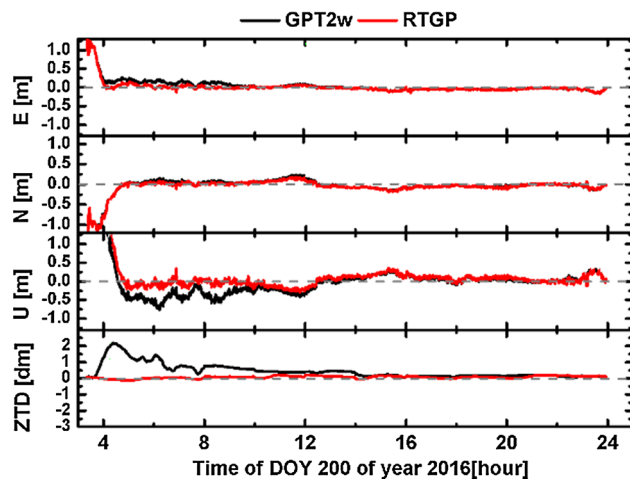


Fig. 11 BDS PPP solutions at station CHUN in DOY 200 of year 2016

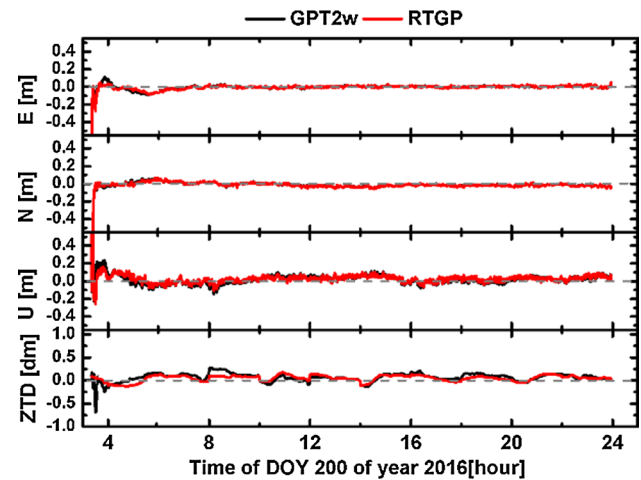


Fig. 13 BDS/GPS combined PPP solution at station CHUN in DOY 200 of year 2016

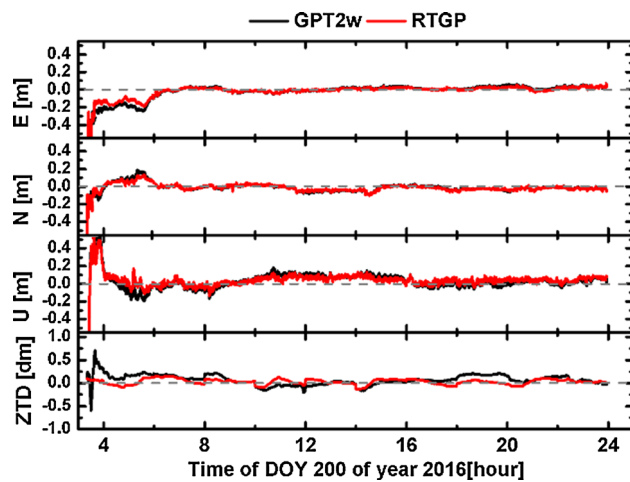


Fig. 12 GPS PPP solutions at station CHUN in DOY 200 of year 2016

66.7, 6.7, 14.6 and 95.8% in East, North, Up direction and the ZTD, respectively. Concerning the GPS-only solution, the improvement is 26.3, 30.0, 40.0 and 58.8%, respectively. For the BDS/GPS combined PPP, no apparent improvement is obtained with the RTGP model. This means that we can obtain a better solution with enough observations independent of the ZTD model, because the TrDOP of the BDS/GPS combined solution is so small that the ZTD can be initialized rapidly and has little influence on the positioning.

In order to quantify the impacts of the RTGP model on the kinematic PPP performance, two weeks' data (DOY 022–028 and DOY 199–205 of year 2016) are processed. The first week is in winter, while the other is in summer. From the above analysis, we find that the RTGP model has almost no effect on the combined PPP solution because the ZTD estimation could be rapidly initialized. We only processed the BDS-only and GPS-only PPP with all the NBASS stations

as shown with green circles in Fig. 2. On the other hand, the PPP performance is affected by the satellite geometry and it is shown that the HDOP, VDOP and TrDOP of the stations vary with time in Figs. 8 and 9. In order to fully evaluate the contributions of the ZTD model on the PPP solution, the PPP is re-initialized (cold start) four times per day. Because the RTGP model is simulated in real-time mode and is re-initialized at UTC 0:00 each day to ensure the accuracy of the RTGP model at the beginning, the first PPP initialized time is set to UTC 02:00.

The statistics of the positioning errors in horizontal and vertical directions are made at the 68% confidence level and the convergence time is determined when the accuracy in the horizontal and the vertical directions is better than 0.2 m, respectively. Figures 14 and 15 present the BDS-only PPP and the GPS-only PPP convergence time series, respectively.

The results shown in Fig. 14 indicate that the BDS PPP with the RTGP model performs better than with the GPT2w model in both periods, especially in the vertical direction. The corresponding convergence time for each re-initialization is listed in Table 6. This shows that the BDS PPP performance varies in different time windows. The improvement is the most significant when the PPP is initialized at UTC 06:00 in summer (July). The horizontal convergence time with the RTGP model declines by 8 min (5.8%) while the vertical convergence time declines by 50 min (50%). On the contrary, when the PPP restarts at UTC 02:00 (July), the improvement by the RTGP model is 2.5 and 20.8% in the horizontal and vertical direction, respectively. It should be noted that the convergence time when re-initialized at UTC 18:00 (Jan.) and UTC 06:00 (July) is much longer than that when the PPP is re-initialized at other times with the GPT2w model, this means that the BDS satellite geometry is poor on average

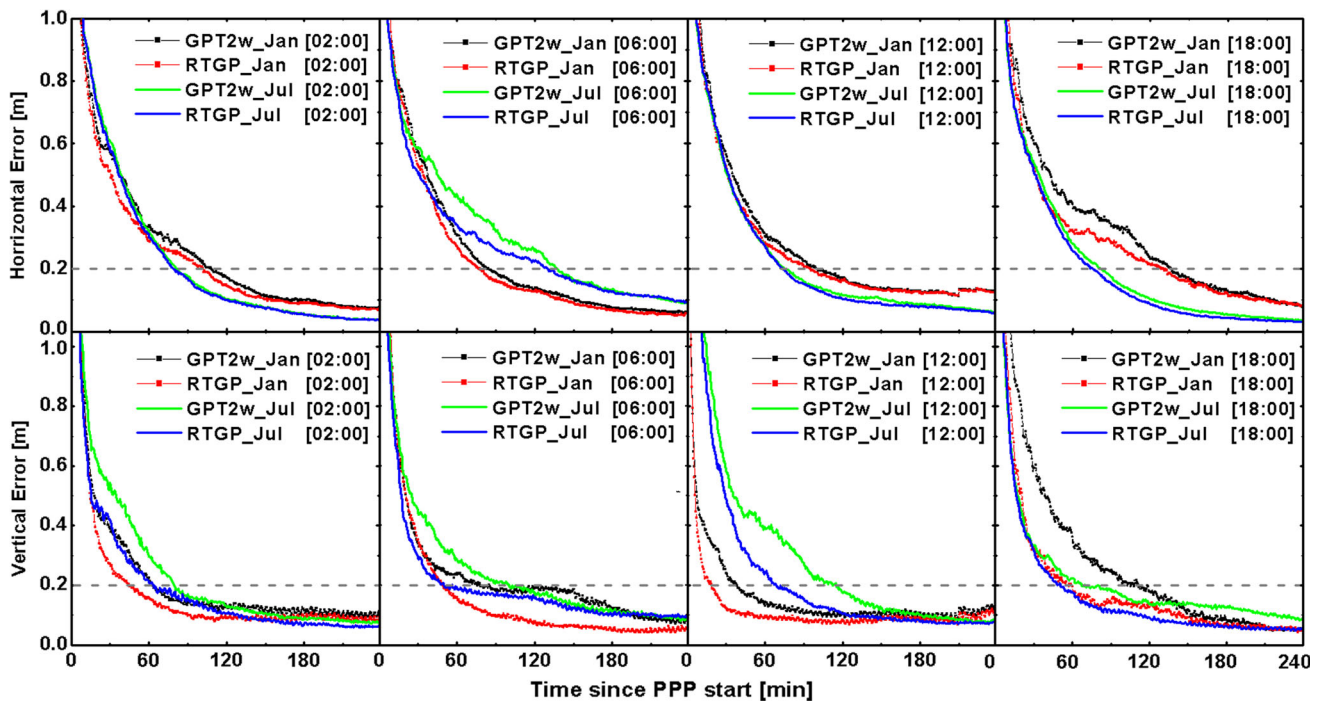


Fig. 14 BDS real-time kinematic PPP positioning errors at the 68% confidence level

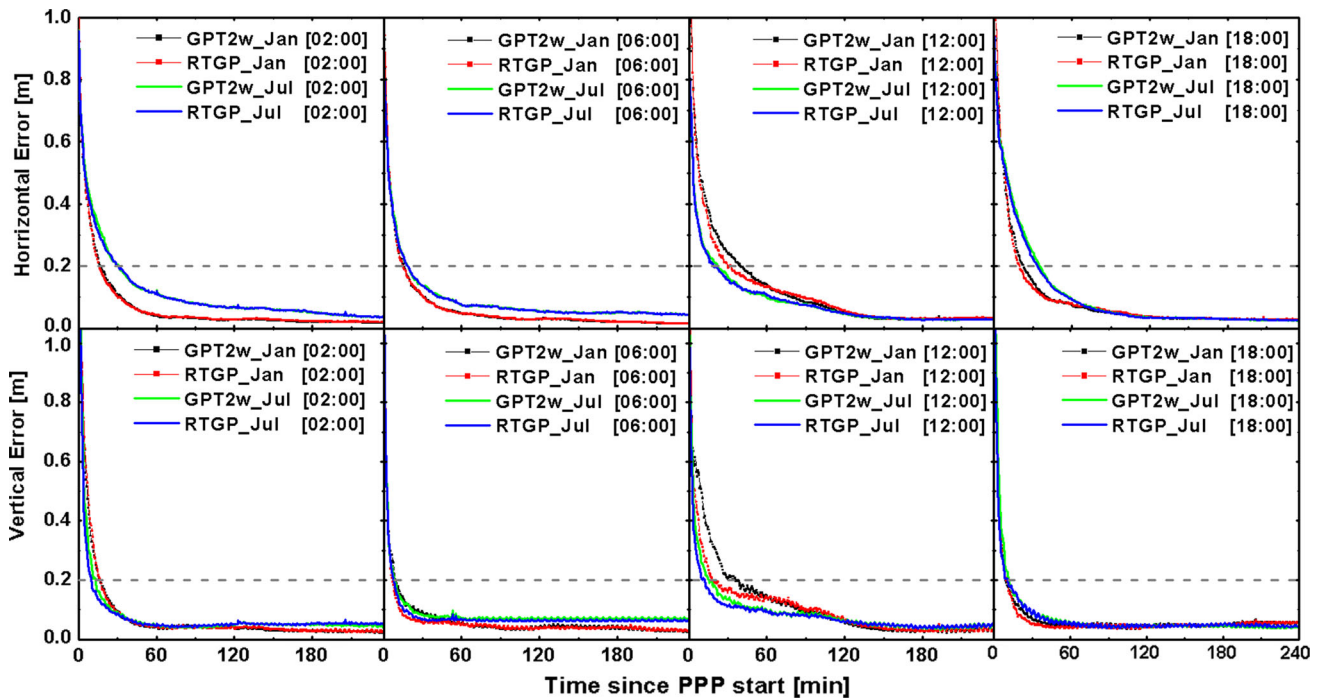


Fig. 15 GPS real-time kinematic PPP positioning errors at the 68% confidence level

at these times, and that the improvement by the RTGP model is more significant than at other times.

Regarding the GPS PPP augmented with the RTGP model, a similar conclusion is reached as with BDS PPP, but the improvement of convergence is less significant. The

most notable improvement is at the time when the PPP is re-initialized at UTC 12:00 (Jan.) and the improvement percentage is 17.1 and 42.0% in the horizontal and vertical directions, respectively. When the GPS PPP is re-initialized at UTC 06:00 (July), there is no improvement in the horizon-

**Table 6** BDS real-time kinematic PPP convergence time (min) at 68% level

	GPT2w_Jan.		RTGP_Jan.		GPT2w_July		RTGP_July	
	Hor.	Vert.	Hor.	Vert.	Hor.	Vert.	Hor.	Vert.
02:00	109.0	64.5	103.5	46.5	81.0	79.5	79.0	63.0
06:00	85.0	79.5	78.5	51.0	138.0	100.0	130.0	50.0
12:00	101.5	40.0	91.5	20.5	76.0	115.5	74.5	69.0
18:00	137.5	104.5	130.5	57.0	81.5	68.0	75.5	51.0

**Table 7** GPS real-time kinematic PPP convergence time (min) at 68% level

	GPT2w_Jan.		RTGP_Jan.		GPT2w_July		RTGP_July	
	Hor.	Vert.	Hor.	Vert.	Hor.	Vert.	Hor.	Vert.
02:00	18.5	18.5	17.5	18.5	31.0	13.5	30.5	10.0
06:00	18.5	11.0	16.5	8.5	18.5	8.5	18.5	8.0
12:00	41.0	34.5	34.0	20.0	22.5	15.5	19.5	10.5
18:00	24.5	10.5	21.5	10.5	36.5	12.0	33.0	11.0

tal direction from introducing the RTGP model, and the only improvement is 5.9% in the vertical direction (Table 7).

Concerning the results of different periods (summer and winter), the average improvement of four time windows (UTC 02:00, 06:00, 12:00 and 18:00) in winter (Jan.) for BDS-only PPP is 6.9 and 39.5% in horizontal and vertical direction, respectively, while the average improvement is about 4.4 and 34.0% in summer (July). For the convergence improvement of GPS-only PPP, the average improvement in horizontal and vertical direction is 11.4 and 16.2% in winter (Jan.), while the average improvement is 6.1 and 18.1% in summer (July).

In general, the RTGP model can effectively improve the kinematic PPP convergence performance in the vertical direction, but the improvement is not significant in the horizontal direction. When the PPP initialization with the GPT2w model is relatively short, the improvement from introduction of the RTGP model is not significant, which means that the contribution of the RTGP model on multi-GNSS combined PPP performance will be not notable compared to the GNSS PPP (BDS-only or GPS-only PPP).

## 5 Conclusions and outlook

In this contribution, the accuracy of zenith tropospheric delay (ZTD) calculated by the GPT2w model in China is evaluated with GNSS observations in year 2016. It is quite diverse in different seasons, the accuracy performance in winter is the best among the four seasons and the accuracy in summer and autumn is worse than that in spring and winter. The average root mean square (RMS) is about 3.6 cm when compared to ZTDs calculated from about 100 GNSS sites. However, the daily maximum RMS can reach more than 12 cm, which means that the blind model is not reliable for real-time appli-

cations at the centimeter level. By modeling the zenith wet delay (ZWD) with a tropospheric grid point model based on the GPT2w model, a tropospheric model, which is applicable in real-time applications, is established, we call it real-time tropospheric grid point (RTGP) model. It can provide high-accuracy ZTD for users. Compared with the local model with optimal fitting coefficients, the RTGP model is more suitable for wide-area troposphere modeling. Similar to results with the GPT2w model, the accuracy of the RTGP model in this study also shows different performance in different seasons, with the average RMS in spring and winter better than that in summer and autumn. The average accuracy of all four seasons of the RTGP model is about 1.2 cm. On the other hand, the daily maximum RMS of the RTGP model is significantly less than that of the GPT2w model.

In the processing of the RTGP model, the calculated ZWD at different altitudes should be converted to the same height. In this study, we convert the ZWD to the mean ETOPO5-based height used in the GPT2w model. While exploring the benefits of the GPT2w model, we combine the method of Dousa and Elias (2014) and the decrease factor of water vapor pressure and the temperature lapse rate provided by GPT2w model and introduce a modified parameter to solve for the uniformity of ZWD at any altitude up to 10 km. The results show that the tropospheric model with this method performs better than that with the water vapor scale height. By introducing the modified parameter, the practicality and applicability of the real-time ZTD can be greatly improved. Potentially inclusion in the GPT2w model of the exponential decay of ZWD with height, introduced by Dousa and Elias (2014), could improve the GPT2w performance. This requires further study.

By introducing the concept of dilution of precision (DOP) with respect to troposphere, the effect of ZTD estimation on PPP solution of different satellite navigation systems, includ-

ing BDS-only, GPS-only and BDS/GPS combined PPP, is analyzed. It shows that the estimation of ZTD mainly affects the positioning in the vertical direction, which results from the high correlation between the ZTD and height. When the satellite geometry is poor, the PPP estimation system is severely ill-conditioned, the accuracy in the vertical direction and ZTD estimation is always terrible, and the result is a long convergence time. In order to solve this problem, the RTGP model is adopted with a strong constraint on the PPP solution. The convergence performance of BDS PPP and GPS PPP with the GPT2w and the RTGP model, respectively, is compared. The results show that the convergence performance is improved significantly after introduction of the RTGP model, especially for BDS PPP. It is reasonable that the improvement for BDS is more significant than that for GPS, because the BDS satellite geometry is always poorer than that of GPS, and the DOP varies relatively slowly.

It must be stressed that the orbit and clock products used in this study are MGEX final products. The accuracy of the RTGP model, and the PPP performance augmented by the RTGP model, need further verification with real-time orbit and clock products. We will develop a real-time GNSS positioning system with the national GNSS reference network in China and test the performance of real-time PPP with the augmented RTGP model in future work.

**Acknowledgements** This work is funded by State Key Research and Development Programme (2016YFB0501802) and supported by the National Nature Science Foundation of China (No. 41374034).

## References

- Ahmed F, Clavovic P, Teferle FN et al (2016) Comparative analysis of real-time precise point positioning zenith total delay estimates. *GPS Solut* 20(2):187–199
- Aske J, Nordius H (1987) Estimation of tropospheric delay for microwaves from surface weather data. *Radio Sci* 22(3):379–386. <https://doi.org/10.1029/RS022i003p00379>
- Blewitt G, Hammond WC, Kreemer C, Plag HP, Stein S, Okal E (2009) GPS for real-time earthquake source determination and tsunami warning systems. *J Geod* 83(3):335–343
- Böhm J, Schuh H (2004) Vienna mapping functions in VLBI analyses. *Geophys Res Lett* 31:L01603. <https://doi.org/10.1029/2003GL018984>
- Böhm J, Werl B, Schuh H (2006a) Troposphere mapping functions for GPS and very long baseline interferometry from European Centre for Medium-Range Weather Forecasts operational analysis data. *J Geophys Res* 111:B02406. <https://doi.org/10.1029/2005JB003629>
- Böhm J, Niell A, Tregoning P, Schuh H (2006b) Global mapping function (GMF): a new empirical mapping function based on numerical weather model data. *Geophys Res Lett* 33:L07304. <https://doi.org/10.1029/2005GL025546>
- Böhm J, Heinkelmann R, Schuh H (2007) Short note: a global model of pressure and temperature for geodetic applications. *J Geod* 81(10):679–683
- Böhm J, Möller G, Schindelegger M, Pain G, Weber R (2015) Development of an improved empirical model for slant delays in the troposphere (GPT2w). *GPS Solut* 19(3):433–441
- Caissy M, Agrotis L, Weber G, Hernandez-Pajares M, Hugentobler U (2012) Coming soon: the international GNSS real-time service. *GPS World* 23(6):52–58
- Chen Q, Song S, Heise S et al (2011) Assessment of ZTD derived from ECMWF/NCEP data with GPS ZTD over China. *GPS Solut* 15(4):415–425
- Collins JP, Langley RB (1997) A tropospheric delay model for the user of the wide area augmentation system. Department of Geodesy and Geomatics Engineering, University of New Brunswick, Fredericton
- Davis JL, Herring TA, Shapiro II, Rogers AEE, Elgered G (1985) Geodesy by radio interferometry: effects of atmospheric modeling errors on estimates of baseline length. *Radio Sci* 20(6):1593–1607
- de Oliveira Jr PS, Morel L, Fund F, Legros R, Monico JFG, Durand S, Durand F (2017) Modeling tropospheric wet delays with dense and sparse network configurations for PPP-RTK. *GPS Solut* 21(1):237–250
- Dousa J, Elias M (2014) An improved model for calculating tropospheric wet delay. *Geophys Res Lett* 41(12):4389–4397
- Dow JM, Neilan RE, Rizos C (2009) The international GNSS service in a changing landscape of global navigation satellite systems. *J Geod* 83(3–4):191–198
- Elosegui P, Ruis A, Davis JL, Ruffini G, Keilm SJ, Bürki B, Kruse LP (1998) An experiment for estimation of the spatial and temporal variations of water vapor using GPS data. *Phys Chem Earth* 23(1):125–130
- Gu S, Shi C, Lou Y, Liu J (2015) Ionospheric effects in uncalibrated phase delay estimation and ambiguity-fixed PPP based on raw observable model. *J Geod* 89(5):447–457
- Hadas T, Bosy J (2015) IGS RTS precise orbits and clocks verification and quality degradation over time. *GPS Solut* 19(1):93–105
- Hopfield HS (1969) Two-quartic tropospheric refractivity profile for correcting satellite data. *J Geophys Res* 74:4487–4499
- Ibrahim HE, El-Rabbany A (2011) Performance analysis of NOAA tropospheric signal delay model. *Meas Sci Technol* 22(11):115107
- Janssen V, Ge L, Rizos C (2004) Tropospheric corrections to SAR interferometry from GPS observations. *GPS Solut* 8(3):140–151
- Kouba J (2008) Implementation and testing of the gridded Vienna Mapping Function 1 (VMF1). *J Geod* 82(4–5):193–205
- Kouba J (2009) A guide to using International GNSS Service (IGS) products. <http://igsceb.jpl.nasa.gov/igsceb/resource/pubs/UsingIGSProductsVer21.pdf>
- Lagler K, Schindelegger M, Böhm J, Krásná H, Nilsson T (2013) GPT2: empirical slant delay model for radio space geodetic techniques. *Geophys Res Lett* 40(6):1069–1073
- Li X, Zhang X, Ge M (2011) Regional reference network augmented precise point positioning for instantaneous ambiguity resolution. *J Geod* 85(3):151–158
- Liu J, Ge M (2003) PANDA software and its preliminary result of positioning and orbit determination. *Wuhan Univ J Nat Sci* 8(2B):603–609. <https://doi.org/10.1007/BF02899825>
- Lu C, Li X, Nilsson T, Ning T, Heinkelmann R, Ge M, Glaser S, Schuh H (2015) Real-time retrieval of precipitable water vapor from GPS and BeiDou observations. *J Geod* 89(9):843–856
- Lu C, Zus F, Ge M, Heinkelmann R, Dick G, Wickert J, Schuh H (2016) Tropospheric delay parameters from numerical weather models for multi-GNSS precise positioning. *Atmos Meas Tech* 9(12):5965
- Lu C, Li X, Zus F, Heinkelmann R, Dick G, Ge M, Wickert J, Schuh H (2017) Improving BeiDou real-time precise point positioning with numerical weather models. *J Geod* 91:1019. <https://doi.org/10.1007/s00190-017-1005-2>

- Niell AE (1996) Global mapping functions for the atmosphere delay at radio wavelengths. *J Geophys Res Solid Earth* 101(B2):3227–3246
- Onn F, Zebker HA (2006) Correction for interferometric synthetic aperture radar atmospheric phase artifacts using time series of zenith wet delay observations from a GPS network. *J Geophys Res Solid Earth* 111(B9)
- Pace B., Pacione R, Sciarretta C, Bianco G (2015) Computation of zenith total delay correction fields using ground-based GNSS. In: Sneeuw N, Novák P, Crespi M, Sansò F (eds) VIII Hotine-Marussi symposium on mathematical geodesy. International association of geodesy symposia, vol 142. Springer, Cham
- Saastamoinen J (1972) Atmospheric correction for the troposphere and stratosphere in radio ranging satellites. *Use Artif Satell Geod* 247–251
- Shi J, Xu C, Guo J, Gao Y (2014) Local troposphere augmentation for real-time precise point positioning. *Earth Planets Space* 66(1):1–13
- Shi J, Xu C, Li Y, Gao Y (2015) Impacts of real-time satellite clock errors on gps precise point positioning-based troposphere zenith delay estimation. *J Geod* 89(8):747–756
- Takeichi N, Sakai T, Fukushima S, Ito K (2010) Tropospheric delay correction with dense GPS network in L1-SAIF augmentation. *GPS Solut* 14(2):185–192
- Wilgan K, Hadas T, Hordyniec P, Bosy J (2017) Real-time precise point positioning augmented with high-resolution numerical weather prediction model. *GPS Solut* 21:1341. <https://doi.org/10.1007/s10291-017-0617-6>
- Yao Y, Xu C, Shi J, Cao N, Zhang B, Yang J (2015) ITG: a new global GNSS tropospheric correction model. *Sci Rep* 5:10273. <https://doi.org/10.1038/srep10273>
- Yao Y, Peng W, Xu C, Cheng S (2017) Enhancing real-time precise point positioning with zenith troposphere delay products and the determination of corresponding tropospheric stochastic models. *Geophys J Int* 208(2):1217–1230
- Yu C, Penna NT, Li Z (2017) Generation of real-time mode high-resolution water vapor fields from GPS observations. *J Geophys Res Atmos* 122(3):2008–2025
- Zumberge JF, Heflin MB, Jefferson DC, Watkins MM, Webb FH (1997) Precise point positioning for the efficient and robust analysis of GPS data from large networks. *J Geophys Res Solid Earth* 102(B3):5005–5017